Auger transition rates for metastable states of antiprotonic helium $\mathrm{He}^+ \bar{p}$

V. I. Korobov* and Isao Shimamura†

The Institute of Physical and Chemical Research (RIKEN), Hirosawa, Wako, Saitama 351-01, Japan
and The Institute of Theoretical Atomic and Molecular Physics, Harvard-Smithsonian Center for Astrophysics,
*60 Garden Street, Cambridge, Massachusetts 02138*

The rates of Auger transitions of antiprotonic helium $^4\mathrm{He}^+\bar{p}$ and $^3\mathrm{He}^+\bar{p}$ are calculated by using a variational scattering method with an elaborate three-body trial function. The shift of the energy levels of these systems due to the coupling with the Auger-decay channels is also obtained from this calculation. Thus an improvement is made over the previously calculated nonrelativistic energies. Together with the relativistic corrections calculated elsewhere, the theoretical transition wavelength between the states $(n,l)=(37,34)$ and $(38,33)$ of $^4\mathrm{He}^+\bar{p}$, for example, is significantly improved to be 713.593 nm, which compares well with the experimental value 713.578 ± 0.006 nm. The calculated Auger lifetime of the level $(38,33)$ is 3.2 ps, as compared with the value 4.1 ± 0.2 ps deduced from the measured line broadening. Auger rates are calculated also using Fermi's golden-rule formula with a regular Coulomb function with no phase shift for the Auger electron. The results agree fairly well with the accurate variational results. [S1050-2947(97)05912-X]

PACS number(s): 36.10.−k, 32.80.Hd

I. INTRODUCTION

Recently measured time spectra of decay products after the stopping of antiprotons $\bar{p}$ in helium clearly showed delayed components, and revealed the existence of extremely long-lived $\bar{p}$; about 3% of the stopped $\bar{p}$ live as long as a few microseconds as compared with a lifetime of some picoseconds of most $\bar{p}$ [1]. These long-lived $\bar{p}$ states have been observed both in $^4\mathrm{He}$ and $^3\mathrm{He}$ [2], but not in any other material studied, and are considered to be due to a mechanism [3] similar to that for long-lived kaons and pions in helium already known from bubble-chamber experiments in the 1960s [4].

The scenario in the independent-particle picture is the following. Most of the $\bar{p}$ stopped in helium in the process

$$\mathrm{He} + \bar{p} \rightarrow \mathrm{He}^+ \bar{p} + e^- \tag{1}$$
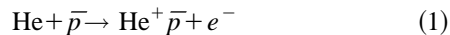
occupy highly excited orbitals in $\mathrm{He}^+\bar{p}$, with principal quantum numbers n around $n^* = \sqrt{M^*/m_e} \simeq 38$, where M^* is the reduced mass between $\bar{p}$ and helium. These $\bar{p}$ cascade down to lower and lower orbitals by the emission of an Auger electron, by radiative transitions, and by energy and angular-momentum transfer in collisions of $\mathrm{He}^+\bar{p}$ with ambient He atoms, and eventually decay in the intra-atomic encounter with the helium nucleus either in a high-n s state or in a low-n state. The neutrality of $\mathrm{He}^+\bar{p}$ and the considerable energy difference between sublevels l with the same n prevent prompt collisional deexcitation and collisional Stark mixing, unless the density of He atoms is extremely high. The radiative transitions from high-n levels are also slow, i.e., of the order of microseconds for n around 30 to 50 (see, e.g., Ref. [5]).

In fact, these $\mathrm{He}^+\bar{p}$ states are not true bound states, but are resonance states in the sense that the electron can acquire from $\bar{p}$ a large enough energy $\Delta\mathcal{E}$ to be emitted as an Auger electron without an external perturbation:

$$(\mathrm{He}^+\bar{p})_{nl} \rightarrow (\mathrm{He}^{2+}\bar{p})_{n'l'} + e^-. \tag{2}$$
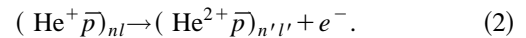
The resultant ion $\mathrm{He}^{2+}\bar{p}$ undergoes rapid collisional Stark mixing because of the degeneracy of sublevels of this hydrogenic ion. The (internal) Auger process (2) is fast for most $(\mathrm{He}^+\bar{p})_{nl}$, but is strongly suppressed for high n, nearly circular ($l \simeq n-1$) orbits, for which the condition of large enough $\Delta\mathcal{E}$ (and hence large enough $\Delta n = n' - n$) automatically excludes small-Δl transitions; note that the Auger process occurs efficiently only for small Δl ($= l' - l$), i.e., only for small angular-momentum transfer to the electron, since an electronic wave function with high angular momentum l_e (greater than about 2) would have a small value in the region of the $\bar{p}$ wave function, and would lead to inefficient energy exchange between $\bar{p}$ and the electron.

Thus the long-lived $\bar{p}$ are considered to be those that are captured into high-n, nearly circular states. The Auger rates are crucial in distinguishing between long- and short-lived $\bar{p}$, and in determining the fraction of the former among all stopped $\bar{p}$. The Auger rates are also indispensable to a study of the whole cascade process.

Subsequent experiments [6,7] used a new technique of a laser-induced transition from a long-lived or metastable parent state to a daughter state that ought to be short lived, i.e., ought to have a high Auger rate. If the laser frequency matches the transition energy, a spike is observed in the delayed component in the time spectrum of decay products at the time when the laser is shot, because of an abrupt increase in the number of short-lived $\mathrm{He}^+\bar{p}$. This technique allows direct measurements of transition wavelengths with a high relative accuracy of some ppm. If the Auger rate of the daughter state is very high, its Auger width may exceed the laser bandwidth, and may be determined experimentally

---

*On leave from Joint Institute for Nuclear Research, 141980 Dubna, Russia.

†Permanent address: The Institute of Physical and Chemical Research (RIKEN), Hirosawa, Wako, Saitama 351-01, Japan.

from the broadening of the line profile of the spike intensity as a function of the laser wavelength, as was indeed done recently [7]. This technique has been further developed in a few different ways, e.g., a double-resonant laser-induced transition from a long-lived to a short-lived state via an intermediate long-lived state [8], and the use of impurity hydrogen molecules to shorten the lifetime of otherwise metastable states and to observe new transitions inaccessible by the original laser-induced transition technique [9]. The Auger rates of $He^+\bar{p}$ states near the borderline between long- and short-lived states play a significant role in the processes occurring in these experiments.

In spite of the importance of the Auger rates of $He^+\bar{p}$, there has not been much effort devoted to accurate calculations of them until recently. The early calculation for some circular orbitals by Russell [10] was based on Fermi's golden rule, with simple wave functions, and with the $\bar{p}$-electron Coulomb interaction chosen as the transition operator. The unpublished work by Ohtsuki, quoted in Refs. [11] and [12], uses more accurate wave functions. Recently, Fedotov, Kartavtsev, and Monakhov [13] and Révai and Kruppa [14] used improved open-channel wave functions representing the final state of the Auger process and fairly elaborate bound-state-type wave functions representing the initial state; the difference between the full Hamiltonian H and the initial-state energy ε_r causes the Auger transition in their approaches.

Since an Auger-allowed state of $He^+\bar{p}$ is a resonance state, which is a continuum state, its energy E_r and the Auger decay width Γ (which is related to the Auger rate λ by $\lambda = \Gamma/\hbar$) are defined as the position and the width of a resonance in the scattering process

$$e^- + He^{2+}\bar{p}. \qquad (3)$$

If one assumes Born-Oppenheimer (BO) separation of the electronic motion from the relative He^{2+}-$\bar{p}$ motion, which is a fairly good approximation for high-n, high-l states, the resonance states turn into molecule-type bound states [5,15,16], which may be called BO states. The kinetic-energy operator for the He^{2+}-$\bar{p}$ motion introduces two kinds of nonadiabatic effects. The first is the coupling with different bound BO states. This effect was taken into account in detail in a previous work using an elaborate analytic variational trial function, leading to a convergence of eigenvalues ε_r of the Hamiltonian matrix within $\sim 10^{-7}$ a.u. [17]. The other effect is the nonadiabatic coupling with continuum or electron-emission channels, which leads both to an Auger process and to a shift $\Delta E = E_r - \varepsilon_r$ of the metastable level. This latter effect of coupling with continuum may be studied by a scattering-type approach to process (3).

In this work we apply to the scattering problem (3) the Kohn variational method with an elaborate trial function similar to the one used in Ref. [17], but augmented by terms representing an Auger-decay channel; only a single channel that contributes most to the Auger rate is taken into account, and hence the only scattering parameter to be considered is the phase shift.

Fermi's golden rule is a good approximation if the correct transition operator is used, and if an accurate and consistent set of initial and final wave functions for the Auger transition are used, as is evident from the Feshbach projection-operator formalism for the resonance parameters [18]. Furthermore, the regular Coulomb function may be used for the Auger electron to a good approximation if the background phase shift is small. Therefore, we also try this simplified Fermi-golden-rule approach, and compare the results with those from the Kohn variational method.

II. FERMI'S GOLDEN RULE

The Fermi golden rule used here for the rate of Auger transition from a given initial bound state Ψ_r with an energy ε_r to a final continuum state Ψ_A reads

$$\Gamma = 2\pi\rho(\varepsilon_r)|\langle\Psi_A|H-\varepsilon_r|\Psi_r\rangle|^2, \qquad (4)$$

where H is the three-body Hamiltonian, and $\rho(\varepsilon)$ is the density of final states per energy ε. In early papers, the operator $H-\varepsilon_r$ was often replaced by the Coulomb interaction between $\bar{p}$ and the electron. The present work, however, avoids this approximation.

A. Initial state of Auger transition

The initial-state wave function $\Psi_r(\mathbf{R},\mathbf{r})$ is expanded in terms of molecule-type basis functions of $\mathbf{R}$, the position vector of $\bar{p}$ with respect to He^{2+}, and $\mathbf{r}$, the position vector of the electron with respect to the center of mass of $\bar{p}$ and He^{2+}. A state with the total orbital angular momentum L, its projection M onto the space-fixed quantization axis, and the total spatial parity η may be written as

$$\Psi_M^{L\eta}(\mathbf{R},\mathbf{r}) = \sum_{m=0}^{L} F_m^{L\eta}(R,r,\theta)\mathcal{D}_{Mm}^{L\eta}(\Phi,\Theta,\varphi), \qquad (5)$$

where

$$\mathcal{D}_{Mm}^{L\eta}(\Phi,\Theta,\varphi) = \left[\frac{2L+1}{16\pi^2(1+\delta_{0m})}\right]^{1/2}[D_{Mm}^L(\Phi,\Theta,\varphi)$$
$$+ \eta(-1)^{L-m}D_{M,-m}^L(\Phi,\Theta,\varphi)] \qquad (6)$$

are the symmetrized Wigner D functions; R, r, and θ are the magnitudes of and the angle between the vectors $\mathbf{R}$ and $\mathbf{r}$; and Φ, Θ, and φ are the Euler angles of a moving body-fixed frame connected with the three-body configuration as follows: The z' axis lies along $\mathbf{R}$, and the y' axis lies in the plane of $\mathbf{R}$ and $\mathbf{r}$. The components $F_m^{L\eta}(R,r,\theta)$ are labeled by the subscript $m = 0, 1, 2, \ldots$ corresponding to the σ, π, δ, $\ldots$ states in the Born-Oppenheimer approximation, and defining the projection of the total orbital angular momentum onto the z axis of the body-fixed frame.

Each function $F_m^{L\eta}$ is expressed as a linear combination [17]

$$F_m^{L\eta} = \sum_{n_1 n_2 n_3} c_{n_1 n_2 n_3} u_{n_1 n_2 n_3}^{(m)}(R,\xi_e,\eta_e)$$

$$= [(\xi_e^2-1)(1-\eta_e^2)]^{m/2}R^m\exp\{-(\alpha+\beta\xi_e)R\}$$

$$\times \sum_{n_1 n_2 n_3} c_{n_1 n_2 n_3}R^{n_1}\xi_e^{n_2}\eta_e^{n_3} \qquad (7)$$

of square-integrable functions of R and spheroidal coordinates $\xi_e = (r_a + r_b)/R$ and $\eta_e = (r_a - r_b)/R$, r_a and r_b being the distances of the electron from the helium nucleus and from the antiproton. Here α and β are nonlinear variational parameters. The linear variational parameters $c_{n_1 n_2 n_3}$, and hence the wave function Ψ_r in Eq. (4), and the corresponding energy value ε_r are determined according to the Rayleigh-Ritz method, i.e., by diagonalizing the Hamiltonian matrix; see Eq. (15) in Sec. III. Although the states of our concern are not true bound states, some lowest eigenvalues are expected to show a rapid ''asymptotic convergence,'' unless too many m components are included in expansion (5). The dependence of the eigenenergies on the number of m components included was studied in Ref. [17], and indeed a rapid convergence was observed; the three-component approximation already turned out to be highly accurate.

B. Auger-electron emission channels

We consider the final state of the Auger transition in which the system $He^{2+}\bar{p}$ is left in a hydrogenic state $\chi_{n'l'}(R)$. Thus we write the continuum wave function in a single-channel form

$$\Psi_A(\mathbf{R},\mathbf{r}) = \psi_{kl_e}(r)\chi_{n'l'}(R)\{Y_{l'} \otimes Y_{l_e}\}_{LM}(\hat{\mathbf{R}},\hat{\mathbf{r}}), \qquad (8)$$

where the angular eigenfunction $\{Y_{l'} \otimes Y_{l_e}\}_{LM}(\hat{\mathbf{R}},\hat{\mathbf{r}})$ is obtained by coupling $\mathbf{l}'$ and $\mathbf{l}_e$ into $\mathbf{L}$. Since the Auger rate is the highest for the smallest possible value of the electronic orbital angular momentum l_e, as explained in Sec. I, we choose only an electronic channel satisfying the condition $l_e = |L - l'|$. Note that, for this choice, the spatial parity $\eta = (-1)^{l' + l_e}$ of the final state is the same as for the initial state, as it should be. Wave functions $\psi_{kl_e}(r)$ of the Auger electron of various levels of accuracy may be considered. For our calculations using Fermi's golden rule (4), we choose the simplest form, namely, $(kr)^{-1}F_{l_e}(kr; -m_e/k)$ involving the regular Coulomb function F_{l_e}, with no scattering phase shift; k is the wave number of the Auger electron. In other words, we choose for Ψ_A in Eq. (4) the function

$$\mathcal{F}(\mathbf{R},\mathbf{r}) = \frac{1}{kr}F_{l_e}(kr; -m_e/k)\chi_{n'l'}(R)\{Y_{l'} \otimes Y_{l_e}\}_{LM}(\hat{\mathbf{R}},\hat{\mathbf{r}}). \tag{9}$$

The normalization of this wave function is such that $\rho(\varepsilon) = 2m_e k/\pi$ as in the case of the free wave.

In Sec. III we use another, similar function

$$\mathcal{G}(\mathbf{R},\mathbf{r}) = (1 - e^{-\alpha' r})^{l_e + \beta' + 1}\frac{1}{kr}G_{l_e}(kr; -m_e/k)\chi_{n'l'}(R)$$

$$\times \{Y_{l'} \otimes Y_{l_e}\}_{LM}(\hat{\mathbf{R}},\hat{\mathbf{r}}), \tag{10}$$

defined in terms of the irregular Coulomb function G_{l_e} and a factor (involving artificial parameters α' and β') for cutting off the singular part of G_{l_e} near the origin. Since this cutoff factor tends to unity as $r \to \infty$, a linear combination of $\mathcal{F}$ and $\mathcal{G}$ would represent a nonzero phase shift.

Naturally, functions (9) and (10) in the atomic representation are expressed in terms of the Jacobi coordinates $(\mathbf{R},\mathbf{r})$. The angular function $\{Y_{l'} \otimes Y_{l_e}\}_{LM}(\hat{\mathbf{R}},\hat{\mathbf{r}})$, however, is expressible as a linear combination of the symmetrized Wigner D functions (6), the coefficients being functions only of the variable θ (see Appendix A). Therefore, these functions may be treated on the same footing as the molecular representation (5).

III. VARIATIONAL SCATTERING APPROACH

More accurate calculations are possible by applying variational methods for scattering to process (3) [19]. For this purpose we adopt a variational trial function

$$\Psi_v = \phi_1 + K\phi_2 + \sum_{j=3}^{N+2} c_j \phi_j, \tag{11}$$

where

$$\phi_1 = \mathcal{F}(\mathbf{R},\mathbf{r}), \quad \phi_2 = \mathcal{G}(\mathbf{R},\mathbf{r}), \tag{12}$$

and where $\{\phi_j\}$ for $j \geq 3$ are square-integrable basis functions $u_{n_1 n_2 n_3}^{(m)}(R,\xi_e,\eta_e)\mathcal{D}_{Mm}^{L\eta}(\Phi,\Theta,\varphi)$ of the same form as are used for calculating Ψ_r for Fermi's golden rule. The coefficients K and $\{c_j\}$ are variational parameters, the former having the meaning of the tangent of the phase shift δ for electron scattering (3). The variational procedure may be described by introducing matrices M, A, and B, whose elements are defined by

$$M_{ij} = \langle \phi_i | H - \varepsilon | \phi_j \rangle \quad \text{for} \quad i,j \geq 1,$$

$$A_{ij} = \langle \phi_i | H | \phi_j \rangle, \quad B_{ij} = \langle \phi_i | \phi_j \rangle \quad \text{for} \quad i,j \geq 3.$$

We also define a matrix $M_0 = A - \varepsilon B$ and vectors $\mathbf{w}_1$ and $\mathbf{w}_2$ of length N composed of matrix elements M_{i1} and M_{i2} for $i \geq 3$.

The variationally optimized phase shift δ_v is determined by the condition that Eq. (11) satisfies the Schrödinger equation in the subspace of functions spanned by $\{\phi_j\}_{j \geq 2}$ [19]. In other words, we demand that the Schrödinger equation projected onto this subspace be satisfied. This leads to a system of coupled linear equations

$$\mathbf{w}_1 + \mathbf{w}_2 K + M_0 \mathbf{c} = 0,$$

$$\tag{13}$$

$$M_{21} + M_{22}K + \mathbf{w}_2^T \mathbf{c} = 0$$

for K, and the vector $\mathbf{c}$ composed of $\{c_j\}$. The optimized value of the tangent of the phase shift is calculated by

$$\tan\delta_v = K + \mathbf{c}^T M_0 \mathbf{c}. \tag{14}$$

This method is referred to as the Kohn variational method. A similar method, in which the roles of ϕ_1 and ϕ_2 are interchanged, is called the inverse-Kohn method, and provides a variationally optimized $\cot\delta_v$.

Resonance structures appear in δ_v close to matrix eigenvalues ε_r defined by

$$A\mathbf{x}_r = \varepsilon_r B\mathbf{x}_r, \tag{15}$$

i.e., close to the energies of the "bound states" Ψ_r. A fit of δ_v to the Breit-Wigner formula for an isolated resonance would produce a set of resonance position E_r, resonance width Γ, and background (or off-resonance) phase shift δ_b. In general, there is a resonance shift $\Delta E = E_r - \varepsilon_r$ from the energy ε_r of Ψ_r, or of Eq. (15). Note that the coefficient vector $\mathbf{c}$ determined from Eq. (13) is independent of the bound-state vector $\mathbf{x}_r$ in Eq. (15), since $\mathbf{c}$ is determined to optimize *the whole continuum state* (11).

In actual numerical calculations in this paper, we use another procedure nearly equivalent to the Kohn method with the Breit-Wigner fitting. This procedure may be derived by working directly on the matrices M, A, and B, as shown in Appendix B.

IV. CALCULATIONS AND RESULTS

The matrices A and B have been calculated to a high precision using the quadruple precision arithmetic, as described previously [17]. The matrix elements M_{ij} (i or $j = 1,2$) involving Coulomb functions have been evaluated by numerical integration over a three-dimensional configuration space of the internal coordinates with the use of Gaussian quadratures, and the final accuracy of these matrix elements is about five significant digits or higher. This lower accuracy than for A and B causes no problem since all the three quantities ΔE, Γ, and δ_b in Appendix B need to be calculated only to a few significant digits.

Some test calculations using various different values of the cutoff parameters α' and β' in Eq. (10) have been carried out. These tests have resulted in a fixed, empirical choice ($\alpha' = 2$, $\beta' = 15$) for the purpose of stable numerical results.

The antiprotonic helium states that play an important role in the experiments summarized in Sec. I are those molecular states Ψ_r in which by far the main Born-Oppenheimer configuration consists of the 1σ electron orbital and a rovibrational He^{2+}-$\bar{p}$ state (j, v), where the rotational quantum number j is practically the same as L in this paper [5]. In terms of an approximate atomic-type representation (n, l) of the He^{2+}-$\bar{p}$ orbital, the vibrational quantum number v corresponds to $n - l - 1$ [5]. The angular-momentum correspondence reads as $j = l$; note that L is a good quantum number, but j and l are not. Since the common electron orbital 1σ need not be specified explicitly, an Auger transition may be specified by the simplified notation (n,l)→(n',l') as in Eq. (2).

For an Auger electron to be emitted in process (2), the energy of the final state $(He^{2+}\bar{p})_{n'l'}$ must be lower than that of the initial state $(He^+\bar{p})_{nl}$. Figures 1 and 2 of the level diagrams indicate that this energy condition sets a lower limit $(\Delta l)_{min}$ to $\Delta l = l' - l$. This lower limit depends on the initial state. For a particular initial state the Auger process with $\Delta l = (\Delta l)_{min}$ has the highest rate, as was explained in Sec. I. Calculations were carried out only for such transitions.

We studied the dependence of the Auger rates on the number of m components retained in the molecular expansion (5). Table I presents the results from both Fermi's golden rule and the variational method and for some transitions with different values of Δl. The dependence is much
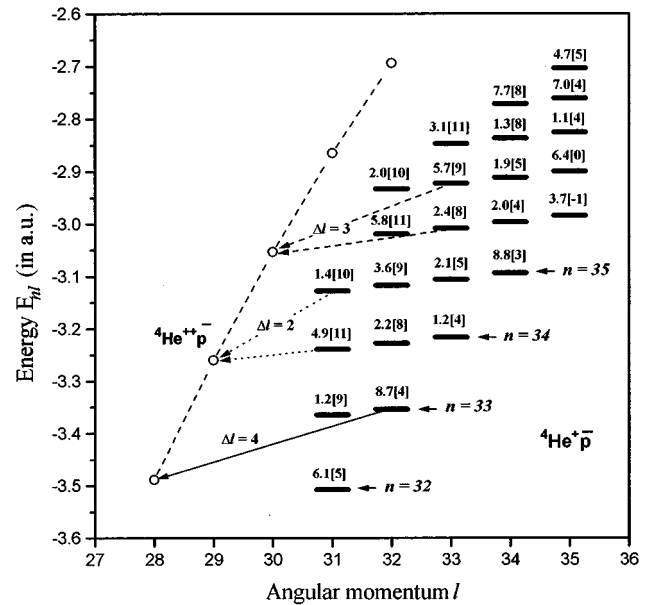

FIG. 1. Energy-level diagram of $^4He^+\bar{p}$ states designated by approximate quantum numbers (n, l); the calculated Auger rate $a[b] = a \times 10^b$ s^{-1} is attached to each level. Open circles represent circular states (n', $l' = n' - 1$) of $^4He^{2+}\bar{p}$. Each arrow connecting a $^4He^+\bar{p}$ level (n, l) and a $^4He^{2+}\bar{p}$ level (n', l') indicates an Auger process with the minimum angular-momentum change $\Delta l = l' - l$ possible for that initial state.

stronger than that of the energy values studied in Ref. [17]. When the number of m components reaches the value of Δl, the Auger rate becomes close to the converged value. While the two methods provide similar results, the variational method is slightly more stable with respect to the change in the basis set.
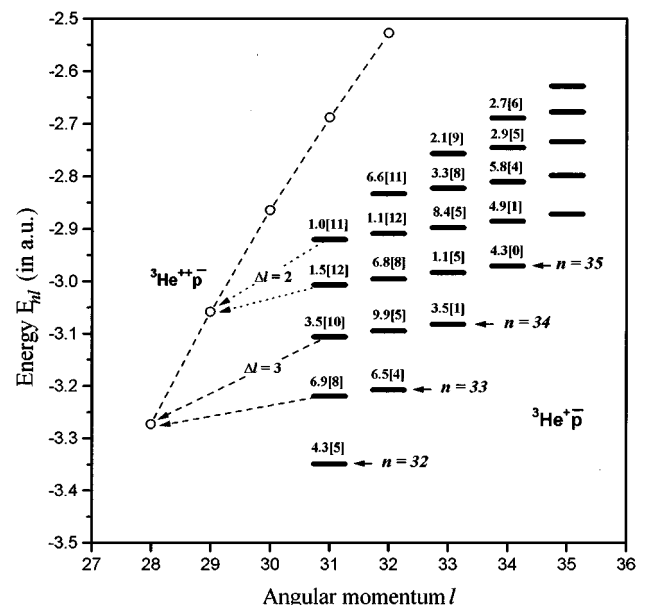

FIG. 2. Same as Fig. 1, but plotted for $^3He^+\bar{p}$ and $^3He^{2+}\bar{p}$; see the caption of Fig. 1.

TABLE I. Dependence of the Auger rates in s^{-1} on the number of m components retained in the molecular expansion (5) for three states (n, l) of ${}^4\mathrm{He}^+\bar{p}$; m_{max} is the maximum value of m retained, and N is the number of basis functions in Eq. (11). FGR: Fermi's golden rule. VM: variational method. $a[b] = a \times 10^b$.

$(n, l, \Delta l)$		(38,33,2)		(39,34,3)		(37,34,4)	
m_{max}	N	FGR	VM	FGR	VM	FGR	VM
0	1200	1.95[9]	1.97[9]	1.76[6]	1.75[6]	4.33[2]	6.14[2]
1	1648	4.01[11]	3.24[11]	1.65[8]	1.65[8]	4.15[4]	4.41[4]
2	1942	3.67[11]	3.08[11]	7.58[8]	7.70[8]	1.26[5]	1.26[5]
3	2158	3.65[11]	3.08[11]	7.95[8]	7.67[8]	1.89[5]	1.85[5]
4	2374					1.87[5]	1.85[5]

A by-product of the variational approach is the background phase shift for electron scattering on $(\mathrm{He}^{2+}\bar{p})_{n'l'}$ in the energy range of the considered resonances. The background phase shift δ_b is as small as $\sim 10^{-2}$ rad or less for the calculated cases where $\Delta l \geq 2$, as is expected from the high centrifugal barrier for an electron with $l_e \geq 2$, which prevents the electron from interacting strongly with $\mathrm{He}^{2+}\bar{p}$. The small δ_b explains the fairly good performance of Fermi's golden rule with the regular Coulomb function for the Auger electron in the final state.

All the states of $\mathrm{He}^+\bar{p}$ calculated in a previous work [17] were treated as bound states. That would lead to some uncertainties in the evaluation of the energy values of the states with Auger width greater than, say, 10^{-7} a.u., since the coupling with Auger-decay channels may not be negligible for these states. Using the present variational scattering approach, improved values of the nonrelativistic energies can be obtained by adding the level shift ΔE to the bound-state energy ε_r. Table II compares the energy ε_r of $({}^4\mathrm{He}^+\bar{p})_{n=38,l=33}$ from the bound-state approach with the shift-corrected energy E_r from the variational-scattering approach, for a few choices of the basis set differing mainly in the components $m \geq 1$. The corrected energy is at least one digit more stable than the uncorrected one, and the correction ranges from 2×10^{-6} to 6×10^{-6} a.u. (with either positive or negative sign), which is of the same order of magnitude as Γ.

The calculated shift-corrected energies E_r, Auger widths Γ, and Auger rates λ are summarized in Table III for ${}^4\mathrm{He}^+\bar{p}$ and in Table IV for ${}^3\mathrm{He}^+\bar{p}$. The typical size of the basis set is $N=2228$ for $\Delta l=2$, $N=2278$ for $\Delta l=3$, and $N=2374$ for $\Delta l \geq 4$. The energies E_r were found to be stable at least to the last digit shown in the tables, and are considered to be accurate to all digits shown. We estimate the errors in the Auger widths from the stability of the numerical results as $\sim 5\%$ for the cases with $\Delta l=2$, $\sim 15\%$ for $\Delta l=3$, $\sim 50\%$ for $\Delta l=4$, and even larger for $\Delta l=5$. There are some exceptions, however, where the convergence was unsatisfactory. Such cases are enclosed in curly brackets in Tables III and IV. Most of the unsatisfactory cases are either for extremely narrow Auger widths, for which the absolute error is actually small, or for states in the upper-right corner in the tables. We suspect that the reason for the latter case might be the overlap of such a resonance with one involving an excited electronic orbital. Tables III and IV clearly demonstrate the extremely strong dependence of the Auger width Γ on Δl; roughly speaking, $\Gamma \simeq 10^{-5} \sim 10^{-7}$ a.u. for $\Delta l=2$, $\Gamma \simeq 10^{-6} \sim 10^{-9}$ a.u. for $\Delta l=3$, $\Gamma \simeq 10^{-10} \sim 10^{-13}$ a.u. for $\Delta l=4$, and $\Gamma < 10^{-13}$ a.u. for $\Delta l=5$. Figures 1 and 2 of the energy-level diagram include the calculated Auger rates.

Table V compares the Auger rates of some selected states obtained in this paper with other theoretical calculations. A thorough comparison reveals that the method of Fedotov et al. [13], which uses basis sets for the initial state including up to 600 atomic-type basis functions and a scattering wave function for an effective potential for the final state, the initial and final wave functions being orthogonal to each other, produces results in agreement with the present values within about 20% except for a few cases. The results of Révai and Kruppa [14], who employ initial-state wave functions of Ref. [17], including up to 1230 terms with $m \leq 2$, also agree well with the present results in most cases. It was found in the present careful numerical investigation that the calculated Auger rates depend strongly on the quality of the wave function. In this sense we believe that our results are the most accurate to date.

A stringent test on the validity of the present variational approach would be a comparison with experimentally determined Auger widths. A candidate for this test found in the literature is the broadening of the line profile for a transition $(n, l) = (37, 34) \rightarrow (38, 33)$ of ${}^4\mathrm{He}^+\bar{p}$ [7]. The full line width at half maximum of 0.067 ± 0.006 nm was much larger than the laser bandwidth of 0.007 nm. This broadening is considered to be due to the Auger width of the daughter state (38,33), since that of the parent state (37,34) is six orders of magnitude smaller according to Table III of this paper. From this broadening the authors of Ref. [7] deduce a lifetime 4.1 ± 0.2 ps of the daughter state, which is to be compared with the value $\lambda^{-1} = 3.2$ ps calculated from Table III. The experimental Auger rate is included in Table V. The mea-

TABLE II. Resonance parameters for ${}^4\mathrm{He}^+\bar{p}(L=33, v=4)$ calculated with four basis sets differing in the size N, and a nonlinear parameter β in Eq. (7) for $F_m^{L\eta}$ with $m \geq 1$. ε_r: eigenvalue of the Hamiltonian matrix in the bound-state approach. E_r: energy-shift corrected variational estimate of the resonance energy. Γ: resonance width. All quantities are in atomic units. $a[b] = a \times 10^b$.

	Bound-state approach	Variational-scattering approach	
	ε_r	E_r	Γ
First set ($N=2388$, $\beta=0.8$)	$-2.847\ 320\ 6$	$-2.847\ 322\ 9$	7.26[−6]
Second set ($N=2270$, $\beta=0.5$)	$-2.847\ 329\ 8$	$-2.847\ 323\ 9$	7.47[−6]
Third set ($N=1934$, $\beta=0.5$)	$-2.847\ 328\ 3$	$-2.847\ 323\ 6$	7.43[−6]
Fourth set ($N=2172$, $\beta=0.4$)	$-2.847\ 329\ 8$	$-2.847\ 323\ 8$	7.45[−6]

TABLE III. Level-shift-corrected nonrelativistic energies E_r (in a.u.), Auger widths Γ (in a.u.), Auger rates λ (in s^{-1}), and the minimum angular-momentum change Δl in Auger transitions for metastable states of ^{4}He$^+\bar{p}$. The antiprotonic atomic-orbital quantum numbers (n, l) are related to the rovibrational quantum numbers (L, v) by $n = v + L + 1$ and $l = L$. The convergence was unsatisfactory for the values in curly brackets. $a[b] = a \times 10^b$.

		$v=0$	$v=1$	$v=2$	$v=3$	$v=4$
$L=31$	E_r	$-3.507\ 634\ 95$	$-3.364\ 651\ 64$	$-3.238\ 577$	$-3.127\ 333$	
	Γ	$1.5[-11]$	$2.9[-8]$	$1.2[-5]$	$\{3.5[-7]\}$	
	λ	$6.1[5]$	$1.2[9]$	$4.9[11]$	$\{1.4[10]\}$	
	Δl	4	3	2	2	
$L=32$	E_r	$-3.353\ 757\ 80$	$-3.227\ 676\ 31$	$-3.116\ 678\ 94$	$-3.019\ 058$	$-2.933\ 090\ 6$
	Γ	$2.1[-12]$	$5.3[-9]$	$9.0[-8]$	$1.4[-5]$	$\{4.8[-7]\}$
	λ	$8.7[4]$	$2.2[8]$	$3.7[9]$	$5.8[11]$	$\{2.0[10]\}$
	Δl	4	3	3	2	2
$L=33$	E_r	$-3.216\ 244\ 20$	$-3.105\ 382\ 64$	$-3.007\ 979\ 02$	$-2.922\ 444\ 12$	$-2.847\ 323\ 8$
	Γ	$2.9[-13]$	$5.0[-12]$	$5.8[-9]$	$\{1.4[-7]\}$	$7.5[-6]$
	λ	$1.2[4]$	$2.1[5]$	$2.4[8]$	$\{5.7[9]\}$	$3.1[11]$
	Δl	4	4	3	3	2
$L=34$	E_r	$-3.093\ 466\ 87$	$-2.996\ 335\ 42$	$-2.911\ 180\ 90$	$-2.836\ 524\ 54$	$-2.771\ 011\ 23$
	Γ	$2.1[-13]$	$4.9[-13]$	$4.6[-12]$	$3.2[-9]$	$1.9[-8]$
	λ	$8.8[3]$	$2.0[4]$	$1.9[5]$	$1.3[8]$	$7.7[8]$
	Δl	5	4	4	3	3
$L=35$	E_r	$-2.984\ 020\ 94$	$-2.899\ 282\ 16$	$-2.825\ 146\ 79$	$-2.760\ 233\ 30$	$-2.703\ 283\ 10$
	Γ	$\{9.0[-18]\}$	$1.6[-16]$	$2.7[-13]$	$1.7[-12]$	$1.1[-11]$
	λ	$\{3.7[-1]\}$	$6.4[0]$	$1.1[4]$	$7.0[4]$	$4.7[5]$
	Δl	5	5	4	4	4

sured line center lies at 713.578 ± 0.006 nm [7], whereas the transition wavelength calculated from Table III (including the effect of the level shifts ΔE) is 713.520 nm. If corrected for the relativistic effect reported elsewhere [20], the theoretical value changes into 713.594 nm, which agrees with experiment within ~ 20 ppm.

In conclusion, we have applied a variational method for scattering to Auger widths Γ and shift-corrected nonrelativistic energies E_r of some states of ^{4}He$^+\bar{p}$ and ^{3}He$^+\bar{p}$ for which the minimum possible angular-momentum change Δl in Auger transitions is 2, 3, 4, or 5. The calculated data on E_r are extremely accurate. Those on Γ should be considerably accurate with a few exceptions, the exceptions being due to the subtlety of the Auger width calculations. Indeed, the calculated Auger width is quite sensitive to the quality of the wave function. The order of magnitude of Γ depends strongly on the value of Δl, and ranges from 10^{-5} to 10^{-17} a.u., the smaller for the larger Δl.

TABLE IV. Level-shift-corrected nonrelativistic energies E_r (in a.u.), Auger widths Γ (in a.u.), Auger rates λ (in s^{-1}), and the minimum angular-momentum change Δl in Auger transitions for metastable states of ^{3}He$^+\bar{p}$. The antiprotonic atomic-orbital quantum numbers (n, l) are related to the rovibrational quantum numbers (L, v) by $n = v + L + 1$ and $l = L$. The convergence was unsatisfactory for the values in curly brackets. $a[b] = a \times 10^b$.

		$v=0$	$v=1$	$v=2$	$v=3$	$v=4$
$L=31$	E_r	$-3.348\ 832\ 11$	$-3.219\ 507\ 18$	$-3.106\ 142\ 2$	$-3.006\ 891$	$-2.919\ 764\ 4$
	Γ	$1.0[-11]$	$1.7[-8]$	$\{8.6[-7]\}$	$3.6[-5]$	$2.5[-6]$
	λ	$4.3[5]$	$6.9[8]$	$\{3.5[10]\}$	$1.5[12]$	$1.0[11]$
	Δl	4	3	3	2	2
$L=32$	E_r	$-3.207\ 672\ 27$	$-3.094\ 450\ 92$	$-2.995\ 404\ 31$	$-2.908\ 857$	$-2.833\ 065\ 6$
	Γ	$1.6[-12]$	$2.4[-11]$	$1.6[-8]$	$\{2.6[-5]\}$	$\{1.6[-5]\}$
	λ	$6.5[4]$	$9.9[5]$	$6.8[8]$	$\{1.1[12]\}$	$\{6.6[11]\}$
	Δl	4	4	3	3	2
$L=33$	E_r	$-3.082\ 114\ 08$	$-2.983\ 373\ 10$	$-2.897\ 192\ 26$	$-2.821\ 962\ 87$	$-2.756\ 217\ 37$
	Γ	$8.4[-16]$	$2.6[-12]$	$2.0[-11]$	$7.9[-9]$	$5.1[-8]$
	λ	$3.5[1]$	$1.1[5]$	$8.4[5]$	$3.3[8]$	$2.1[9]$
	Δl	5	4	4	3	3
$L=34$	E_r	$-2.970\ 628\ 27$	$-2.884\ 912\ 60$	$-2.810\ 261\ 07$	$-2.745\ 174\ 13$	$-2.688\ 292\ 86$
	Γ	$1.0[-16]$	$1.2[-15]$	$1.4[-12]$	$7.1[-12]$	$6.6[-11]$
	λ	$4.3[0]$	$4.9[1]$	$5.8[4]$	$2.9[5]$	$2.7[6]$
	Δl	5	5	4	4	4

TABLE V. Comparison of Auger rates variationally calculated for some states of $^4\mathrm{He}^+\bar{p}$ with other theoretical and experimental results. $a[b]=a\times10^b\ \mathrm{s}^{-1}$.

$(n,l,\Delta l)$	Ohtsuki [a]	Ohtsuki [b]	Fedotov [c]	Révai [d]	Present	Yamazaki [e]
(38,33,2)				2.7[11]	3.1[11]	2.4±0.1[11]
(38,34,3)	8.5[7]	2.2[8]	1.4[8]	1.3[8]	1.3[8]	
(39,34,3)	1.8[9]	2.5[9]		8.3[8]	7.7[8]	
(37,34,4)	2.7[4]	2.9[6]	2[5]	7.4[4]	1.9[5]	
(39,35,4)	6.7[2]	3.4[5]	1.0[5]	2.8[5]	7.0[4]	

[a]Unpublished, quoted in Ref. [11].
[b]Unpublished, quoted in Ref. [12].
[c]Reference [13].
[d]Reference [14].
[e]Experimental: Ref. [7].

ACKNOWLEDGMENTS

APPENDIX A: ATOMIC VS MOLECULAR REPRESENTATION

A relation between the atomic representation (8) and the molecular representation of form (5) may be established by using the formula

$$\{Y_l\otimes Y_{l_e}\}_{LM}(\hat{\mathbf{R}},\hat{\mathbf{r}})=\sqrt{2\pi}\sum_{m=0}^{l_e}G_{ll_e}^{Lm}\mathcal{D}_{Mm}^{L\eta}Y_{l_em}(\theta,0),$$

where the coefficients $G_{ll_e}^{Lm}$ are defined by

$$G_{ll_e}^{Lm}=\left[\left(\frac{2}{1+\delta_{0m}}\right)\left(\frac{2l+1}{2L+1}\right)\right]^{1/2}\langle Lm|l0l_em\rangle$$

in terms of a Clebsch-Gordan coefficient. Thus Eq. (8) may be cast into a form

$$\Psi_A(\mathbf{R},\mathbf{r})=\sqrt{2\pi}\,\psi_{kl_e}(r)\chi_{n'l'}(R)$$
$$\times\sum_{m=0}^{l_e}\mathcal{D}_{Mm}^{L\eta}(\Phi,\Theta,\varphi)G_{l'l_e}^{Lm}Y_{l_em}(\theta,0),$$

which is to be compared with Eq. (5). Equations (9) and (10) may also be written in a similar form.

APPENDIX B: VARIATIONAL PROCEDURE FOR RESONANCE PARAMETERS

Here we sketch the method of calculating resonance parameters, working directly on the matrices and vectors defined in the text. First the inverse matrix M_0^{-1}, for ε close to ε_r of Eq. (15), is represented in a form

$$M_0^{-1}=\overline{M}_0^{-1}+\frac{1}{\varepsilon_r-\varepsilon}\mathbf{x}_r\mathbf{x}_r^T,$$

where $\overline{M}_0^{-1}$ is the inverse matrix of rank $N-1$ in the subspace that is B orthogonal to $\mathbf{x}_r$, and varies slowly with the change in ε. We also introduce quantities

$$\bar{w}_{sr}=\mathbf{x}_r^T\mathbf{w}_s\quad(s=1,2).$$

Solving Eqs. (13) for K, we have

$$K=-\frac{M_{21}-\mathbf{w}_2^TM_0^{-1}\mathbf{w}_1}{M_{22}-\mathbf{w}_2^TM_0^{-1}\mathbf{w}_2}=-\frac{(\varepsilon_r-\varepsilon)G_{21}-\bar{w}_{2r}\bar{w}_{1r}}{(\varepsilon_r-\varepsilon)G_{22}-\bar{w}_{2r}^2},$$

where

$$G_{2s}=M_{2s}-\mathbf{w}_2^T\overline{M}_0^{-1}\mathbf{w}_s\quad(s=1,2).$$

The resonance position E_r and the resonance width Γ are calculated from a pole $E_r-i\Gamma/2$ of the scattering matrix $S=(1+iK)(1-iK)^{-1}$. Retaining only two leading terms in the slowly varying function $\bar{w}_{2r}\bar{w}_{sr}$ of ε near $\varepsilon=\varepsilon_r$ and writing

$$\bar{w}_{2r}\bar{w}_{sr}\simeq\bar{w}_{2r}^0\bar{w}_{sr}^0-(\varepsilon_r-\varepsilon)\left.\frac{d(\bar{w}_{2r}\bar{w}_{sr})}{d\varepsilon}\right|_{\varepsilon=\varepsilon_r}\quad(s=1,2),$$

we find that

$$\Delta E=E_r-\varepsilon_r=-\frac{\bar{w}_{2r}^0(\bar{w}_{1r}^0\bar{G}_{21}+\bar{w}_{2r}^0\bar{G}_{22})}{\bar{G}_{22}^2+\bar{G}_{21}^2},$$

$$\Gamma/2=\frac{\bar{w}_{2r}^0(\bar{w}_{1r}^0\bar{G}_{22}-\bar{w}_{2r}^0\bar{G}_{21})}{\bar{G}_{22}^2+\bar{G}_{21}^2},$$

$$\tan\delta_b=G_{21}/G_{22},$$

where

$$\bar{G}_{2s}=G_{2s}+\left.\frac{d(\bar{w}_{2r}\bar{w}_{sr})}{d\varepsilon}\right|_{\varepsilon=\varepsilon_r}\quad(s=1,2).$$

[1] M. Iwasaki *et al.*, Phys. Rev. Lett. **67**, 1246 (1991).

[2] T. Yamazaki *et al.*, Nature (London) **361**, 238 (1993).

[3] G. T. Condo, Phys. Lett. **9**, 65 (1964).

[4] J. G. Fetkovich and E. G. Pewitt, Phys. Rev. Lett. **11**, 290 (1963); M. M. Block *et al.*, *ibid.* **11**, 301 (1963); M. M. Block, J. B. Kopelman, and C. R. Sun, Phys. Rev. **140**, B143 (1965); J. G. Fetkovich *et al.*, Phys. Rev. D **2**, 1803 (1970).

[5] I. Shimamura, Phys. Rev. A **46**, 3776 (1992).

[6] N. Morita *et al.*, Phys. Rev. Lett. **72**, 1180 (1994); F. Maas *et al.*, Phys. Rev. A **52**, 4266 (1995); H. A. Torii *et al.*, *ibid.* **53**, R1931 (1996).

[7] T. Yamazaki *et al.*, Phys. Rev. A **55**, R3295 (1997).

[8] R. S. Hayano *et al.*, Phys. Rev. A **55**, 1 (1997).

[9] B. Ketzer *et al.*, Phys. Rev. Lett. **78**, 1671 (1997).

[10] J. E. Russell, Phys. Rev. A **1**, 742 (1970).

[11] N. Morita, K. Ohtsuki, and T. Yamazaki, Nucl. Instrum. Methods Phys. Res. A **330**, 439 (1993).

[12] T. Yamazaki, *Atomic Physics 13* (AIP, New York, 1993), p. 325.

[13] S. I. Fedotov, O. I. Kartavtsev, and D. E. Monakhov, Yad. Fiz. **59**, 1717 (1996) [Phys. At. Nucl. **59**, 1662 (1996)].

[14] J. Révai and A. T. Kruppa, Phys. Rev. A (to be published).

[15] P. T. Greenland and R. Thürwächter, Hyperfine Interact. **76**, 355 (1993).

[16] P. T. Greenland, J. S. Briggs, and R. Thürwächter, J. Phys. B **27**, 1233 (1994).

[17] V. I. Korobov, Phys. Rev. A **54**, R1749 (1996).

[18] H. Feshbach, Ann. Phys. (N.Y.) **5**, 357 (1958); **19**, 287 (1962).

[19] R. K. Nesbet, *Variational Methods in Electron-Atom Scattering Theory* (Plenum, New York, 1980).

[20] V. I. Korobov and D. D. Bakalov, Phys. Rev. Lett. **79**, 3379 (1997).